DOE/PC/92176--T1

DE93 013605

THERMODYNAMIC PROPERTIES OF PULVERIZED COAL DURING RAPID HEATING DEVOLATILIZATION PROCESSES

QUARTERLY PROGRESS REPORT

October - December 1992

Prepared by

W.M. Proscia
J.D. Freihaut

United Technologies Research Center
411 Silver Lane
E. Hartford, CT 06108

For

U.S. Department of Energy
Pittsburgh Energy Technology Center

Contract No. DE-AC22-92PC92176

DOE Contracting Officer's Representative

Clifford A. Smith

March 1993

CONTENTS

1.0 Executive Summary

Knowledge of the thermodynamic and morphological properties of coal associated with rapid heating decomposition pathways is essential to progress in coal utilization technology. Specifically, knowledge of the heat of devolatilization, surface area and density of coal as a function of rank characteristics, temperature and extent of devolatilization in the context of rapid heating conditions is required both, for the fundamental determination of kinetic parameters of coal devolatilization, and to refine existing devolatilization sub-models used in comprehensive coal combustion codes.

The objective of this research is to obtain data on the thermodynamic properties and morphology of coal under conditions of rapid heating. Specifically, the total heat of devolatilization, external surface area, BET surface area and true density will be measured for representative coal samples. In addition, for one coal, the contribution of each of the following components to the overall heat of devolatilization will be measured: the specific heat of coal/char during devolatilization, the heat of thermal decomposition of the coal, the specific heat capacity of tars, and the heat of vaporization of tars.

Calibration of the heated grid calorimeter (Task 2) was completed this reporting period. Several refinements to the heated grid apparatus have been implemented which allow quantitative determination of sample heat capacity at high heating rates. In particular, grid temperature calibration, improvement of sample load area measurement techniques, a revised correlation for the heat capacity of the stainless steel grid material, and validation of the analysis procedure using sapphire and anthracite samples have all been completed.

A data analysis protocol has been developed which extracts sample heat capacity measurements from the raw experimental data. The analysis is a two step process: a first order estimate for the sample heat capacity is obtained by invoking the assumption that the power dissipation per unit area of the reference material and sample loaded regions of the grid are equal. The first order estimate for sample heat capacity is then used as input to a transient, 2-D analysis of the grid. The actual grid mass, initial temperature and experimental current data are also required input to the simulation. A grid energy balance code previously developed at UTRC has been extensively modified to allow calculations on sample/reference material loaded grids to be performed. The code also determines a corrected sample heat capacity by calculating the difference in local power dissipation between the reference material and sample loaded areas. The power correction term results in a correction of about 10% to the original, first order estimate for heat capacity. Thus, the power correction is significant and use of this correction improves the accuracy of the heat capacity measurements.

Heat capacity runs using synthetic sapphire standards and an anthracite char sample have been conducted to validate the analysis protocol. Heat capacity measurements for sapphire are within 5% of NIST certified values. Heat capacity measurements for the anthracite char are bracketed on the low side by independent, low heating rate, DSC data and on the high side by the Merrick model for heat capacity. Additional, independent, measurements of the heat capacity of the anthracite char sample will be pursued to complete the validation of the high heating rate measurements. Other inert carbon samples will also be examined for their suitability as reference materials.

In addition to the HG calibration effort, significant progress on Task 5 was completed this quarter. Matched tar and char samples have been generated in the UTRC EFR. Elemental analysis results for the tars and chars are used to determine the extent of reaction. The parent coal and char samples will be used to determine the thermodynamic properties and morphology of coal as a function of extent of reaction.

Task 3, Low Temperature Specific Heat Capacity of Volatile Coal Samples will be initiated immediately using PSOC 1451D as the study coal. Task 10, Morphological Characterization, will be performed under subcontract to the University of Pittsburgh. It is expected that the subcontract will be in place early in the upcoming quarter.

2.0 Introduction and Overview of Technical Objectives

Introduction

Knowledge of the thermodynamic and morphological properties of coal associated with rapid heating decomposition pathways is essential to progress in coal utilization technology. Specifically, knowledge of the heat of devolatilization, surface area and density of coal as a function of rank characteristics, temperature and extent of devolatilization in the context of rapid heating conditions is essential to the fundamental determination of kinetic parameters of coal devolatilization. These same properties are also needed to refine existing devolatilization sub-models utilized in large-scale modeling of coal combustion systems.

In many instances the kinetic analysis of rapid coal devolatilization data acquired in laboratory reactors depends on an assumed set of heat capacity, heat of devolatilization and particle morphology parameters. In other cases, attempts to measure particle temperatures during devolatilization (Refs. 1,2,3) lead to results that are not in agreement either with a priori determinations obtained with energy balance expressions using estimations of thermodynamic properties of coal found in the open literature or inert, carbon-based calibration standards used to calibrate the reactor system. Although it is not always clear if the discrepancies are due to inadequate thermodynamic properties of the particle during devolatilization, particle shape factors, inadequate emittance values or some combination of these factors, it is now apparent that independent determinations of these properties in heating conditions characteristic of disperse phase coal utilization technology is necessary. Moreover, since it is now well-established that the energy transfer rate between an environment and injected coal particles, significantly influences the observable devolatilization response time of the particles (Ref. 4), the independent determination of the specific heat and devolatilization heat of reaction of coal is necessary.

Objective

The objective of this research is to obtain data on the thermodynamic properties and morphology of coal under conditions of rapid heating. Specifically, the total heat of devolatilization, external surface area, BET surface area and true density will be measured for representative coal samples. The coal ranks to be investigated will include a high volatile A bituminous (PSOC 1451D) and a low volatile bituminous (PSOC 1516D). An anthracite (PSOC 1468) will be used as a non-volatile coal reference. In addition, for one coal, the contribution of each of the following components to the overall heat of devolatilization will be measured: the specific heat of coal/char during devolatilization, the heat of thermal decomposition of the coal, the specific heat capacity of tars, and the heat of vaporization of tars.

Project Tasks

The work required to complete the objectives of this investigation has been divided into eleven tasks. Each of these tasks is summarized below. The details of the technical approach have been described previously (Ref. 5).

Task 1 - Project Work Plan

UTRC shall provide the DOE with a detailed Project Plan within 30 days of contract initiation. Work on no other tasks shall proceed until written approval of this plan is obtained by UTRC from the DOE Project Manager. The Project Plan shall include a Management Plan, Milestone Schedule, Status Report, and Cost Plan.

Task 2 - Calibration of the Heated Grid Calorimeter

UTRC shall measure the specific heat of the non-volatile reference coal (anthracite, PSOC 1468) from 25° C to 800° C at heating rates of 1000° C/sec and lower in the heated grid (HG) device. The values will be established relative to NBS calorimeter standards for differential scanning calorimeter (DSC) and differential thermal analysis (DTA) samples. The sensitivity of the heated grid device for determining thermodynamic properties at high heating rates will be established before proceeding with Tasks 3-9.

Task 3 - Low Temperature Specific Heat Capacity of Volatile Coal Samples

UTRC shall measure the specific heat capacity for a minimum of one coal sample over the temperature range of 25° C to 300° C. The measurements will be conducted at heating rates of 1000° C/sec and lower in the UTRC HG.

Task 4 - Heat of Devolatilization of Volatile Coal Samples

UTRC shall measure the heat of devolatilization for a minimum of one coal sample over the temperature range of 25° C to 800° C using heating rates of 1000° C/sec in the calibrated HG. Devolatilization product characteristics will be determined to ensure the devolatilization pathway is that followed in the entrained flow reactor (EFR).

Task 5 - Heat of Thermal Decomposition of Volatile Coal Samples

UTRC shall measure, using the EFR and microbomb calorimeter (MBC), the heat of decomposition for a minimum of one coal sample by: (1) devolatilizing the coal in the EFR, (2) determining the char, tar and gas yields, (3) measuring the tar and char elemental compositions, (4) determining the heat of combustion of the char and tar products using the MBC, (5) estimating the heat of combustion of the gaseous products, and (6) using Hess's and Kirchoff's laws to derive the heat of decomposition.

Task 6 - Specific Heat and Heat of Fusion of Tars from Rapid Heating

UTRC shall measure the specific heat and heat of fusion of tar samples for a minimum of one coal sample over the temperature range from 25° C to 300° C using the HG and tar samples generated in the EFR.

Task 7 - Heat of Vaporization of Tars from Rapid Heating

UTRC shall measure the heat of vaporization of tar samples for a minimum of one coal sample over the temperature range from 300° C to 700° C using the HG and tar samples generated in the EFR.

Task 8 - Specific Heat of Char Samples

UTRC shall measure the specific heat of the coal/char as a function of extent of devolatilization and temperature for a minimum of one coal sample using partially devolatilized samples from the EFR and the HG.

Task 9 - Comparison of Directly Measured Heat of Devolatilization and Thermodynamic Function Determined Value

UTRC shall determine the heat of devolatilization for a minimum of one coal sample based on independent measurements of heat of decomposition (Task 5), specific heat and heat of fusion of tars (Task 6), heat of vaporization of tars (Task 7), and specific heat of coal/chars (Task 3 and Task 8). This value shall be compared and contrasted to the directly measured heat of devolatilization values from 25° C to 800° C obtained in Task 4.

Task 10 - Morphological Characterization of Coal/Char Samples as a Function of Extent of Devolatilization

UTRC shall characterize statistically representative samples of coal/char particles as a function of extent of devolatilization for a minimum of one coal sample. The characterization shall be with respect to combustion related reactivity parameters such as swelling and cenosphere development, CO_2 or O_2 surface areas, and helium (true) density.

Task 11 - Reporting

UTRC shall comply with all required reporting over the 18 month period of the contract.

3.0 Task 2. Calibration of the Heated Grid Calorimeter

The objectives of this task are to calibrate the heated grid apparatus using known heat capacity standards and to determine the sensitivity of the technique. Prior to discussing the details of the calibration effort, the theoretical basis for obtaining heat capacity measurements from the heated grid apparatus will be reviewed (Ref. 5).

3.1 Use of the UTRC-HG as a Calorimeter

The heated grid is to be used to measure the heat capacity of devolatilizing samples at high heating rates. Heat capacity of the unknown sample is determined by reference to a known standard material. The classical DSC procedure is to perform independent measurements for the blank pan, reference material loaded pan and unknown sample loaded pan. The reference and sample loaded runs are then baseline corrected using the blank pan data. The run-to-run variability in grid characteristics, such as blank grid mass and grid-to-electrode electrical contact resistance, would contribute to measurement error if this technique was applied to the heated grid data. In order to eliminate the need for baseline (or blank grid) corrections, the experiments will be performed with both the unknown and reference samples loaded on separate regions of the *same* grid.

First Order Heat Capacity Estimate

A simple energy balance can be used to estimate, as a first order approximation, the heat capacity of the sample from the raw experimental data. Consider the energy balance for the sample and reference loaded areas of the screen only. Both the sample loaded area and the reference loaded area in the proximity of the measurement thermocouples are similar isolated areas on the grid. As a first approximation, the power dissipation per unit area *as a function of time* of both the sample and reference loaded regions *within* these isolated areas are assumed equal,

$$\frac{P_s(t)}{A_s} = \frac{P_r(t)}{A_r} \tag{1}$$

If the thermal inertia of the sample and reference loaded areas are identical, and if the loads are uniformly distributed across the full width of the grid, this relationship should hold exactly. Otherwise, a correction to the equation is required as will be described later. Expanding equation (1) in terms of thermal inertia and heat loss terms gives,

$$\left(m_s C_s + m_g C_g\right)\dot{T}_s + Q_L(T_s) = \left(m_r C_r + m_g C_g\right)\dot{T}_r + Q_L(T_r) \tag{2}$$

where m_s, m_r and m_g are the sample, reference material and grid masses per unit area, respectively; C_s, C_r and C_g are the sample, reference and grid specific heats evaluated at the appropriate temperature; and $Q_L(T_s)$ and $Q_L(T_r)$ are the heat loss rates per unit area of the grid at the sample and reference loaded region temperatures, respectively. Note the implicit assumption that the sample and grid temperature are equal in the sample loaded region. Similarly, the reference material temperature is assumed to be at the grid temperature in the reference loaded region of the grid. Solving equation (2) for sample specific heat:

$$C_s = \frac{(m_r C_r + m_g C_g)}{m_s} \frac{\dot{T}_r}{\dot{T}_s} - \frac{m_g C_g}{m_s} + \frac{\Delta Q_L^{r-s}}{m_s \dot{T}_s} \qquad (3)$$

where ΔQ_L^{r-s} is a heat loss correction due to the difference in temperature between the reference and sample loaded areas at a given time. The sample and reference loaded temperature derivatives are determined by first smoothing the raw temperature data to eliminate noise and then fitting the smoothed data with 3rd order polynomials. The heat loss correction term is evaluated using an empirical correlation for the FHG described previously (Ref. 5). Note that the areas of the grid covered by the sample and reference material enter into the equation through m_s and m_r. The sample and reference material masses and areas must be measured as a function of time.

Improved Estimate of Sample Heat Capacity

If the assumption that the power dissipation of the sample and reference loaded regions are equal is relaxed, then the following equation for sample specific heat results,

$$C_s = \frac{(m_r C_r + m_g C_g)}{m_s} \frac{\dot{T}_r}{\dot{T}_s} - \frac{m_g C_g}{m_s} + \frac{\Delta Q_L^{r-s}}{m_s \dot{T}_s} - \frac{\left(\frac{P_r}{A_r} - \frac{P_s}{A_s}\right)}{m_s \dot{T}_s} \qquad (4)$$

where a term for the difference in *local* power dissipation between the reference and sample loaded areas now appears. One approach for quantifying this term is to perform a transient 2-D calculation of the entire grid area between the electrodes. The grid is discretized into a 2-D mesh and an energy balance is applied to each element accounting for resistive heating, heat loss, and conduction in two dimensions. The influence of the sample heat capacity on the local response of the

grid is included by adding the sample thermal inertia to the appropriate mesh elements in the model. Details of the 2-D model are given in Appendix A.

Given the grid current as a function of time and correlations for grid heat loss, grid resistivity, and grid, reference material and sample heat capacities as a function of temperature, the energy balance model calculates the temperature and electrical resistance of each element. The resistance across the sample-loaded region of the grid, and therefore local voltage drop and power dissipation, can then be determined. Thus, the 2-D model allows an estimate for $\left(P_r / A_r - P_s / A_s\right)$ to be calculated given an assumed sample specific heat. The calculated power dissipation correction term can then be used to determine a corrected heat capacity.

Analysis Protocol For The Determination Of Heat Capacity

The theory described above can be combined into an overall analysis methodology for determining heat capacity at high heating rates using the heated grid apparatus. The analysis protocol for the determination of heat capacity in the heated grid is as follows:

1) Load the grid with known mass of sample "around" T/C 1 and known mass of reference material "around" T/C 2.

2) Run heated grid at 1000°C/s and acquire temperature, voltage, current, and image data.

3) Use image analysis techniques to extract sample & ref. mat'l. loaded areas from raw images. This is performed using "Image" v1.47 S/W from NIH.

4) Perform first order analysis to estimate sample heat capacity. This is accomplished using the "HCAPACITY" code. The analysis uses equation (3) as given previously.

5) Create binary image files which indicate the load/no-load state of each point on the grid. "Image" S/W is also used for this operation. The binary image files are read by the 2-D analysis code and used to apply the boundary conditions to the model.

6) Run 2-D, transient simulation ("GRIDMOD") of the loaded heated grid. Given inputs for grid current vs. time (step 2), sample and reference material load distributions (step 5) and estimated sample heat capacity (step 4), the code calculates the time-varying temperature distribution for the entire grid. Calculated temperatures at the locations of the sample and reference T/C's are compared to experimentally measured values. The difference in power dissipation between the reference material and sample loaded regions of the grid is used to form a corrected sample heat capacity (equation 4). The validity of the simulation is also checked by comparing calculated grid voltage and power to the experimentally measured values.

7) Repeat step 6 using the corrected sample heat obtained therein. Check for agreement between calculated and measured sample temperatures. Our experience to-date indicates that agreement is obtained after only a single iteration of this step.

3.2 Heated Grid Calibration

Several refinements to the heated grid apparatus have been implemented which allow quantitative determination of sample heat capacity at high heating rates. In particular, grid temperature calibration, improvement of sample load area measurement techniques, a revised correlation for the heat capacity of the stainless steel grid material, and validation of the analysis procedure using sapphire and anthracite samples have all been completed and will be described below.

Temperature Calibration

Temperature calibration of the heated grid was completed during this reporting period. Temperature is measured using a 0.002" (50 μm) bead dia. Type-K (Chromel-Alumel) thermocouple spot welded to the grid. The thermocouple signal is amplified by 100X and acquired using a National Instruments 12-bit A/D board. The accuracy of the temperature measurements was examined using OMEGALAQ Temperature Indicating Liquids (OMEGA). The OMEGALAQ liquids have an accuracy of +/- 1% of the rated temperature. A small, thin spot of the indicating lacquer was applied to the grid near the thermocouple. Several trial runs were conducted to determine the appropriate amount of sample which would allow observation of the phase transition without excessively loading the grid. The grid was then heated at 50 °C/sec while recording a magnified and time-coded image of the lacquer onto video tape. The video system has a time resolution of 1/30 sec, corresponding to a temperature measurement resolution of 1.67 °C at the heating rate used. The melting temperature of the lacquer was determined by locating the video frame(s) at the point the phase transition is observed and matching the elapsed time for the frame to the corresponding temperature measured by the data system. Results are as follows:

TABLE I

GRID TEMPERATURE CALIBRATION

OMEGALAQ Rated Temperature (°C)	Measured Temperature (°C)
500	500
704	720
804	784

The determination of the point of melting is somewhat subjective. Even with relatively thin lacquer coatings, thermal lag was evident as the lacquer heated from the edge inward. The point at which the edge of the lacquer undergoes transition was used for the measured temperatures reported here. The measured temperatures above represent an average of three independent determinations of the melting transition. The individual determinations varied by as much as +/- 20 °C. Part of this variability can be explained by the +/-1% accuracy of the OMEGALAQ, but much of it is due to the subjective nature of determining the melting transition from the images.

Sample Area Measurement

The analysis used to determine sample heat capacity from the raw experimental data requires accurate measurement of sample and reference material load areas. Considerable effort was expended to develop an improved method for back lighting the sample. Initial attempts utilizing point light sources, parabolic reflectors and diverging lenses all failed to provide a field of uniform intensity which was dispersed over the required area. Success was achieved with a "light bar" design consisting of a half cylinder dispersion element fed by a light pipe and fiber optic bundle (Fig. 1). The light bar uniformly illuminates the entire width of the grid for a length of 4 cm. The difference in image quality between the new and old systems is shown in Figure 2.

FIGURE 1. LIGHT BAR

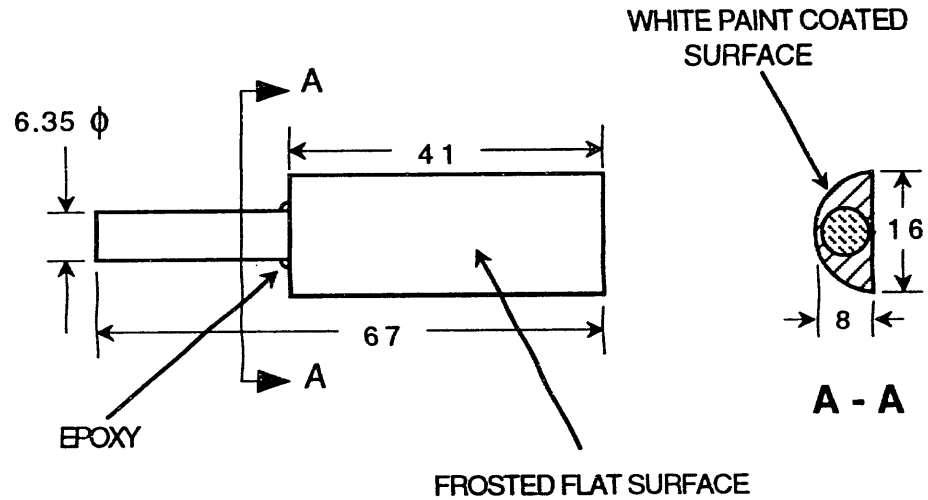

ALL DIMENSIONS IN MM

MATERIALS:
PYREX
WHITE PAINT
EPOXY

FIGURE 2 SAPPHIRE SAMPLE DISPERSED ON THE HEATED GRID

A. ORIGINAL LIGHTING SET-UP

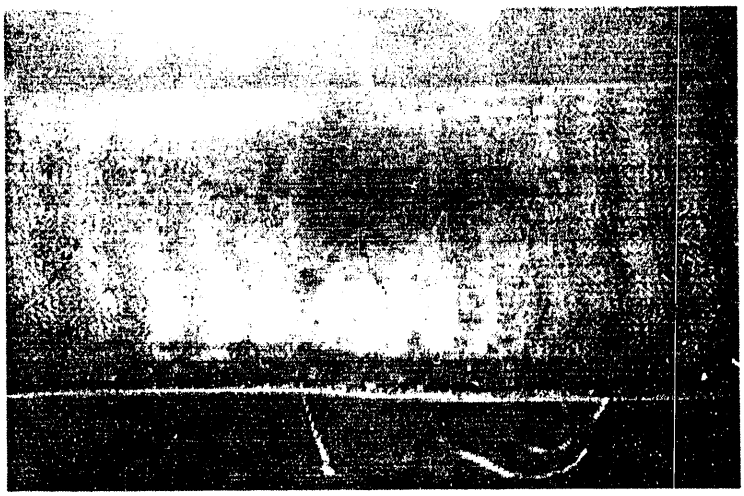

B. IMPROVED, LIGHT BAR SET-UP

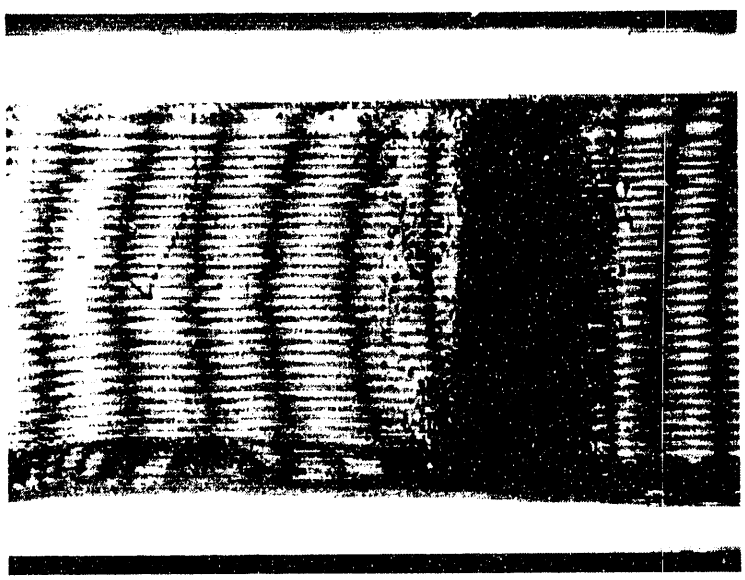

Sapphire Heat Capacity Determinations

The sensitivity and accuracy of the heat capacity measurements were tested by applying the technique to NIST certified sapphire samples with known heat capacity. Several sapphire experiments have been conducted in an effort to develop experimental procedures which result in uniform sample distributions on the grid. An experiment was conducted using a "pocket" to contain the sample. The pocket was formed by spot welding the two folds of the grid together across the width of the grid. The grid was loaded with 26.3 mg of sapphire. The measured sample areas before and after the run are 0.495 and 0.501 cm^2, respectively. (Figs. 3 - 4). The grid was then heated at 1000°C/s to 1300°C. The blank screen temperature reaches 1300°C, whereas the sample loaded T/C temperature peaks at about 550°C. Figure 5 shows the substantially lower temperatures obtained by the sample loaded grid as compared to the blank region of the grid. The effect of the thermal inertia of the sapphire is clearly evident. The large difference in the response of the loaded and blank areas provides ample sensitivity for determining the heat capacity of the sample. In fact, a lower sample loading will be required to allow data to be obtained at higher temperatures. The blank screen temperature cannot be driven any higher without inducing failure of the grid. (The melting point of 304 SS is about 1400°C.)

Unfortunately, the "pocket" technique was found to unacceptable because of difficulties in consistently spot welding the grid without burn-through. Variability in welder output resulted in occasional overheating of the grid resulting in holes in the strand weave pattern. These defects in the grid change the resistance and local current flow at the edge of the sample region and make the analysis of the data considerably more complex. For, this reason the "pocket" technique was abandoned and no further analysis of these runs will be presented.

Eventually, a satisfactory sapphire distribution was obtained by painstaking sample placement and careful handling of the grid during reactor assembly. The nominal sapphire loading for the run was 41 mg/cm^2. Since, the mass loading of a monolayer of sapphire is about 18 mg/cm^2, this represents a sapphire layer about two particle diameters in thickness. The thermal response of the sample will not lag that of the grid appreciably at a heating rate of 1000°C/s. A first order estimate of the heat capacity of sapphire was extracted from the raw data using equation (3) given previously, except that the blank grid material serves as the reference material. The resulting *measured* heat capacity for the sapphire sample is compared with the NIST certified values in Figure 6. Agreement is acceptable considering the difficulty of performing these high heating rate measurements. The measured heat capacity values are within 10% of the NIST certified values over the temperature range from 100 to 500°C. Below 100°C the large relative error in the temperature measurements may be a factor. More important is the deviation at high temperature. It is apparent that the measured heat capacity is not increasing as rapidly with temperature as the NIST certified values. Also shown on the Figure are results calculated using the new heat capacity correlation for stainless steel which will be described below.

Figure 3. Before Run SAPP013

a. Raw Image of Sapphire Sample on Grid

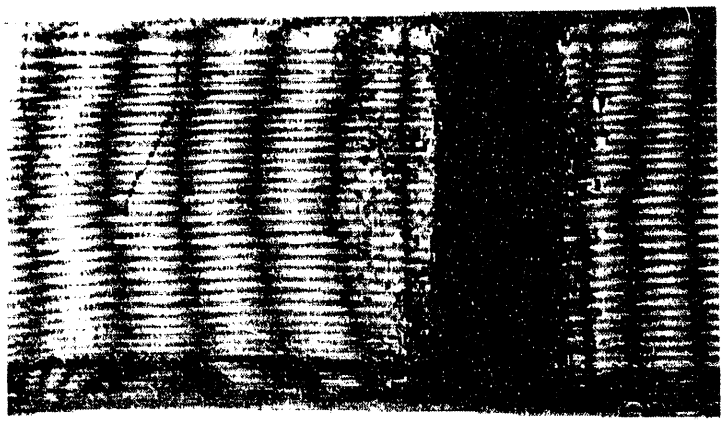

b. Binary Representation of Sample Area

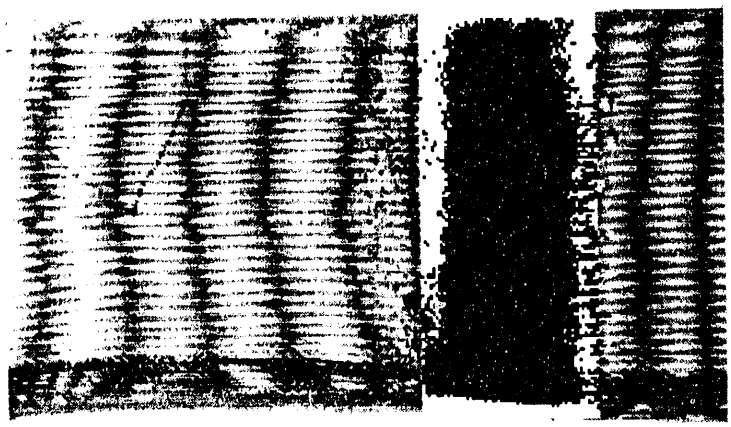

Figure 4. After Run SAPP013

a. Raw Image of Sapphire Sample on Grid

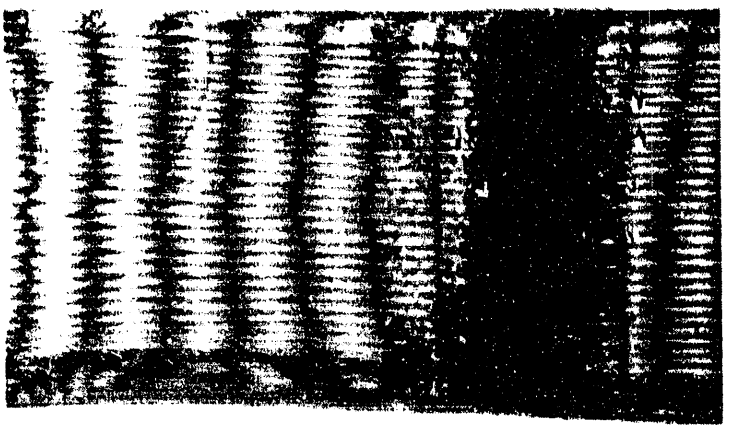

b. Binary Representation of Sample Area

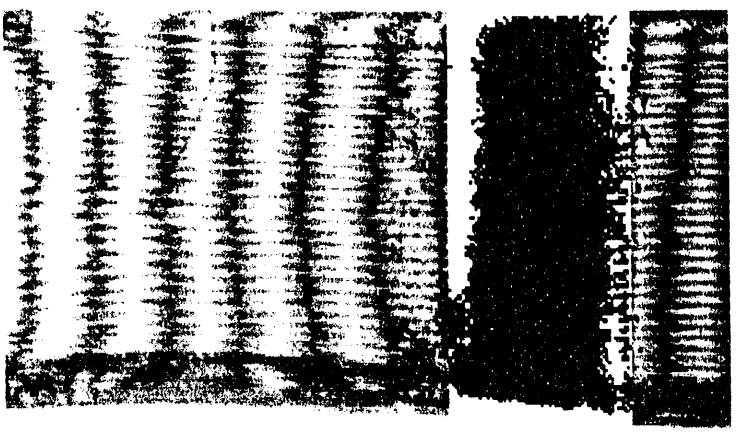

FIG. 5 BLANK AND SAMPLE-LOADED GRID TEMPERATURES - RUN SAPP013

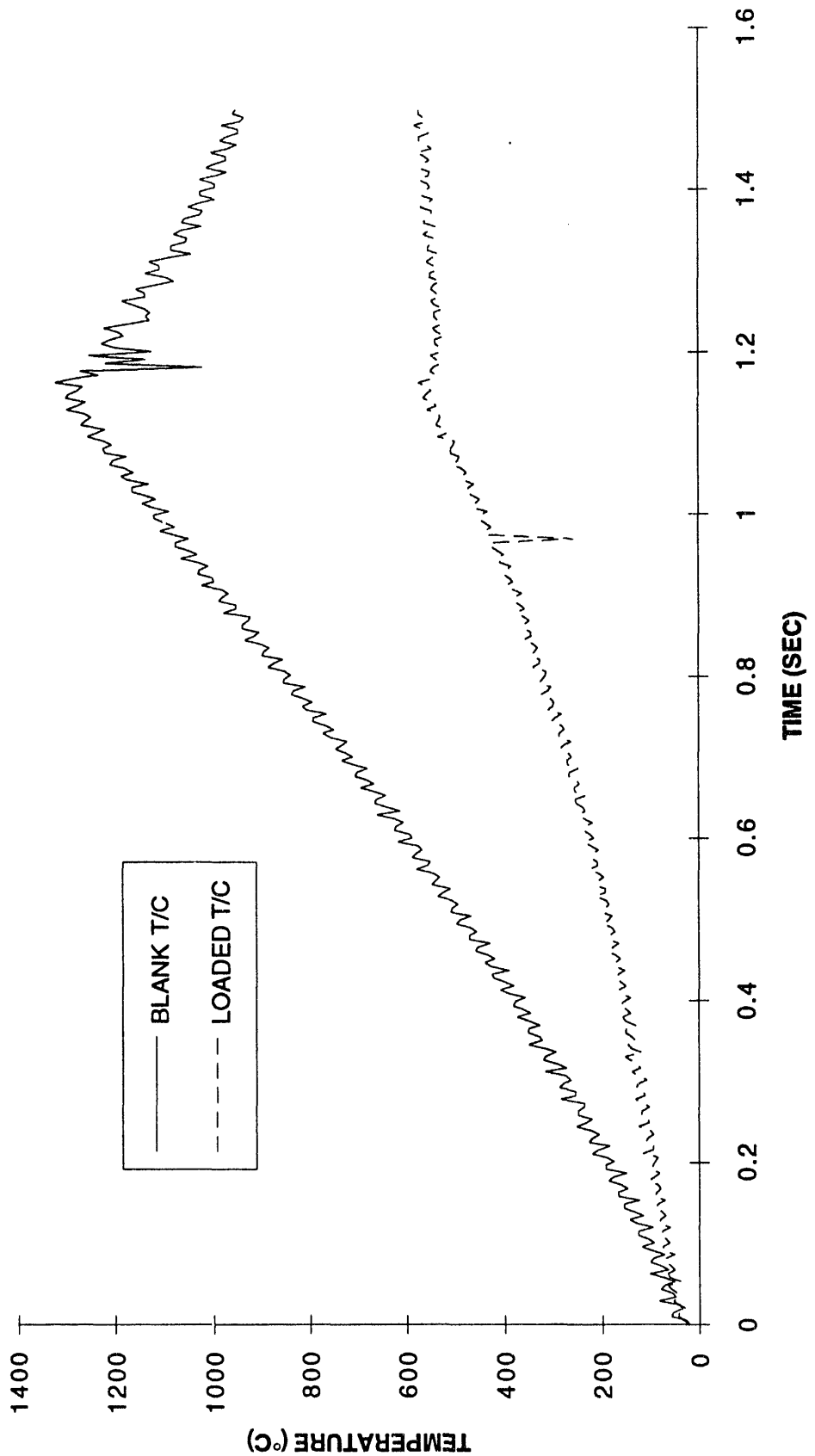

FIG. 6 FIRST ORDER ESTIMATE OF SAPPHIRE Cp
USING ORIGINAL & REVISED STAINLESS STEEL Cp

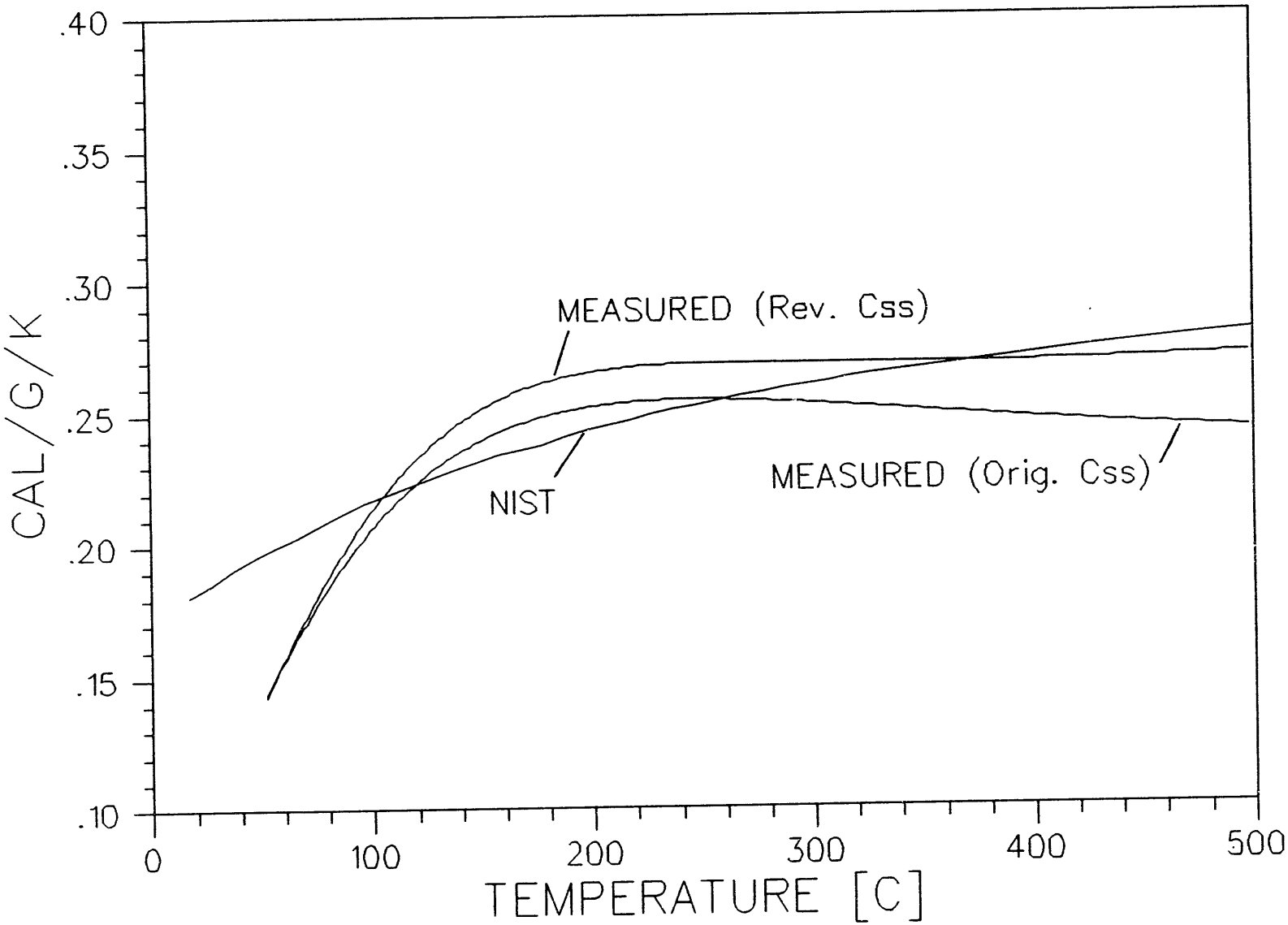

Since the blank grid is used as the reference material for this run, any inaccuracies in the correlation for grid material heat capacity translate directly into errors in the estimated heat capacity of the sample. Also, the large difference in temperature between the sample loaded and blank regions results in a much larger heat loss correction term than would be the case for a sample and reference material loaded run. The heat loss correction becomes significant at a sapphire temperature of only 200°C for this run (blank region temp. is 400°C). Any inaccuracies in the heat loss correlation also result in sample heat capacity measurement errors. Although, it is not possible to determine independent corrections for *both* stainless steel heat capacity and grid heat loss from the sapphire/blank grid experiment, the first order heat capacity analysis technique can be "calibrated" using the sapphire data. Since, an independent empirical heat loss correlation for the grid in its current configuration has been completed (Ref. 5), it will be assumed that this correlation is accurate. The deviation between measured and actual sapphire heat capacity will be attributed entirely to errors in the stainless steel heat capacity data.

Revised Grid Material Heat Capacity Correlation

Both, the first order sample heat capacity estimate and transient, 2-D analysis require as input knowledge of the heat capacity of the grid material as a function of temperature. A correlation of handbook data for 304 stainless steel had been used up to the present time. This correlation was based on a very limited set of data and the fit was rather poor at high temperatures. In addition, heat capacity measurements of sapphire in the heated grid apparatus, which were determined using the stainless steel grid material as the reference, were substantially lower than NIST certified values at high temperature. A revised heat capacity correlation for stainless steel is necessary, and furthermore can be derived from the existing data already obtained in the heated grid.

The sapphire/blank grid experiment was used to estimated the heat capacity of the 304 stainless steel grid material using NIST standard sapphire as the reference material. The existing analysis procedure was inverted to allow calculation of the blank grid heat capacity. The following equation must be solved for the heat capacity of stainless steel at the blank screen temperature, $C_g(T_s)$,

$$C_g(T_s) = \left(C_g(T_r) + \frac{m_r}{m_g} C_r(T_r)\right) \frac{\dot{T}_r}{\dot{T}_s} + \frac{\Delta Q_L^{r-s}}{m_s \dot{T}_s} \qquad (5)$$

where the subscripts "s" and "r" denote the blank and sapphire loaded regions, respectively. Since, the heat capacity of the grid material must be evaluated at both the blank and reference loaded temperatures, an iterative solution procedure is required. The resulting code, "GRIDCP," calculates grid heat capacity from the raw experimental data. Note, that although the maximum sapphire temperature is 500°C, the blank grid temperature about 1100°C in the same run. Thus, this analysis

provides new data for stainless steel heat capacity up to temperatures of 1000°C. The calculated stainless steel heat capacity values are unreliable at low temperatures, but provide improved data at high temperatures. A new heat capacity for correlation has been developed by fitting the original low temperature handbook data and the high temperature data obtained in the heated grid. The original and revised heat capacity correlations for stainless steel are compared in Fig. 7.

The new stainless steel heat capacity correlation was used to repeat the heat capacity analysis for sapphire. The results yield, as expected, somewhat higher values for sapphire heat capacity at high temperatures (Fig. 6). The measured and NIST certified values for sapphire now agree within 5% at high temperatures.

In order to further validate the heated grid calibration a blank heated grid experiment was conducted and analyzed using the full transient, 2-D energy balance calculations. The actual grid mass, initial temperature and experimental current data are used as input to the simulation. The calculated temperatures at the points corresponding to the two T/C locations are compared with experimental temperature data in Figures 8 and 9. There is virtually no error up to 800°C, and above this temperature the calculations overpredict experimental data by about 5%. The overprediction implies that the grid heat capacity correlation is still underestimating the true values at high temperatures. Recall that the measurements described above for sapphire heat capacity were 5% lower than the certified values. Since, the sapphire measurements were obtained using the blank grid as the reference, the 1:1 correspondence between the two sets of results is not surprising. Overall, these results substantiate the assumptions and correlations used in the transient 2-D model.

Anthracite Reference Material Preparation

The final step in the calibration of the heated grid apparatus is to measure the heat capacity of an anthracite coal which will be used as the reference material throughout this investigation. The anthracite, PSOC 1468, was prepared by devolatilizing the sample in an oven at 650°C under nitrogen. Mass loss from the anthracite was approximately 3% under these conditions. The heat capacity of anthracite char was measured in the HG calorimeter and compared with independent determinations performed in a commercial DSC apparatus.

FIG. 7 ORIGINAL AND REVISED STAINLESS STEEL HEAT CAPACITY

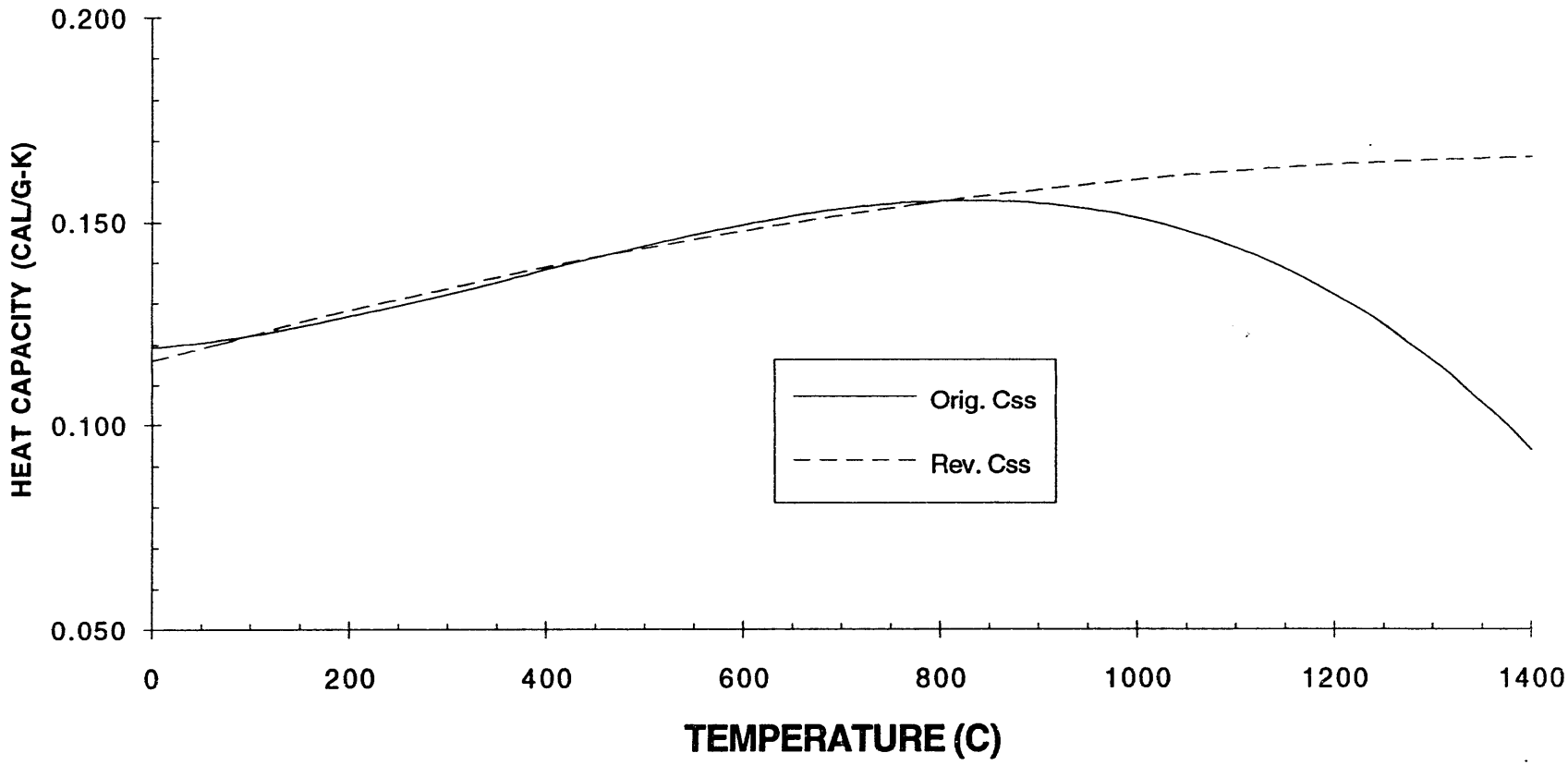

FIG. 8 SAMPLE TEMPERATURES
CALCULATED (LINE) AND EXPERIMENTAL (SYMBOLS)

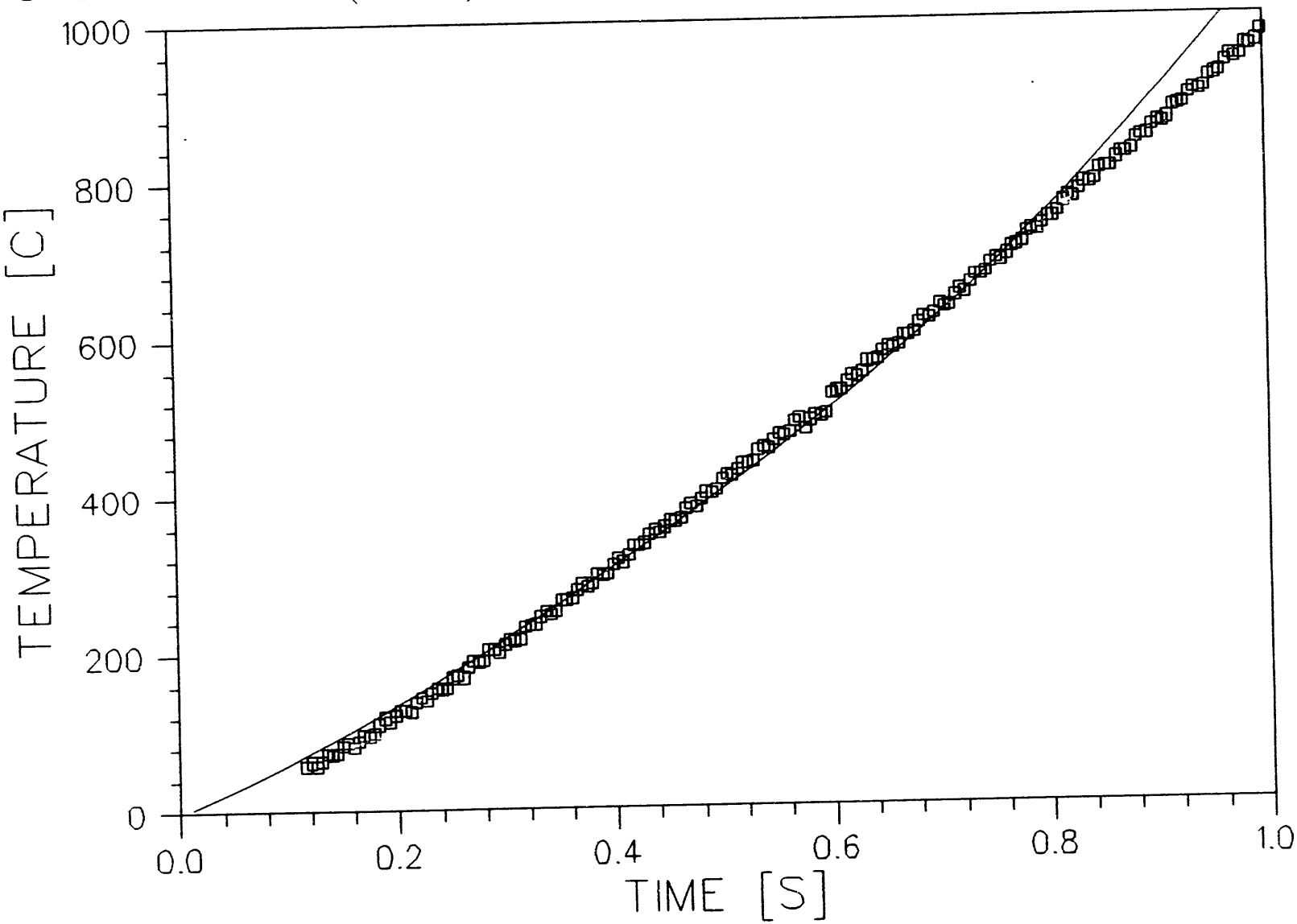

FIG. 9 REFERENCE MATERIAL TEMPERATURES
CALCULATED (LINE) & EXPERIMENTAL (SYMBOLS)

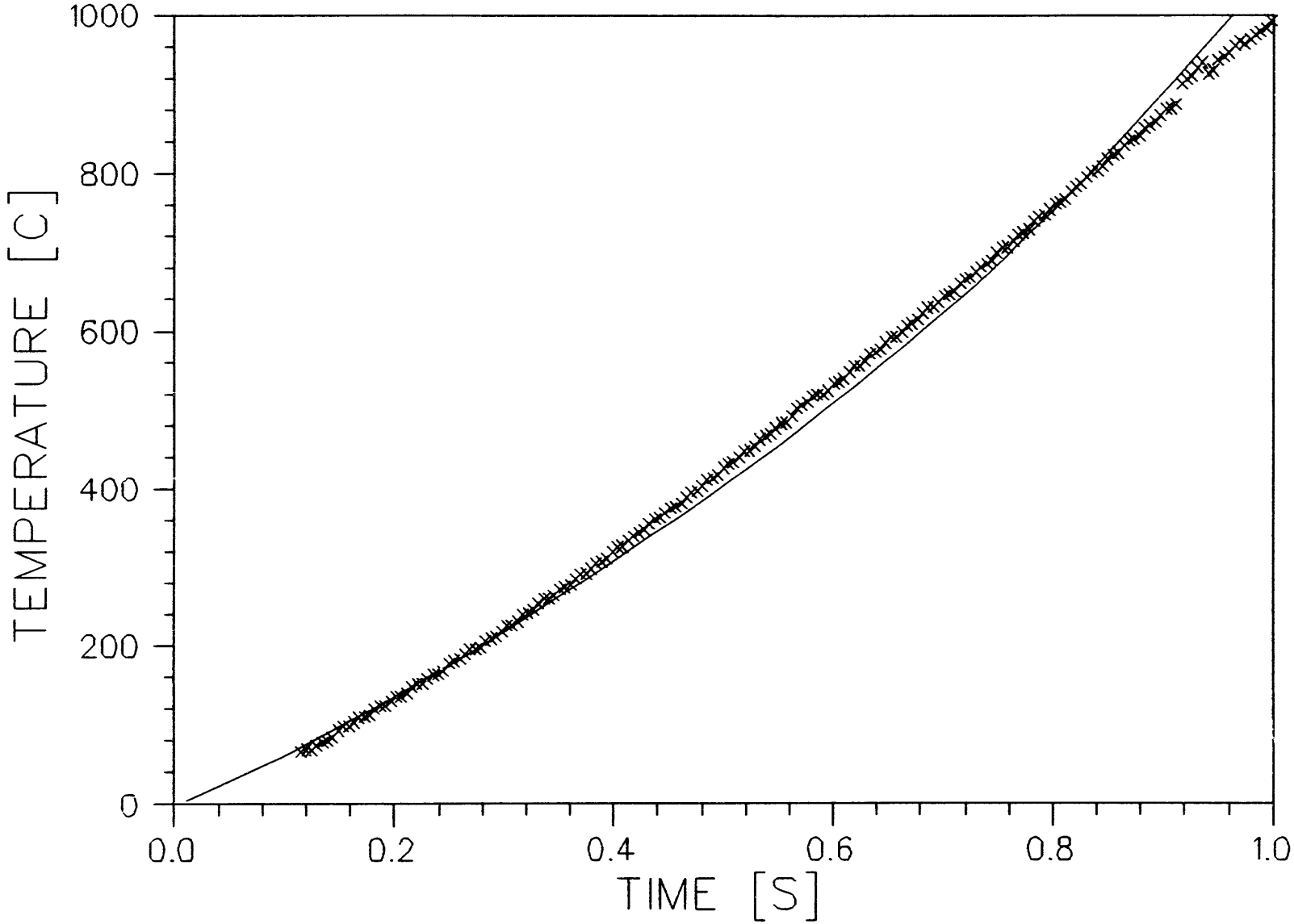

Anthracite Heat Capacity Measurements

The anthracite char sample, generated as described above, was subjected to a series of heated grid runs of progressively higher final temperature (Table II). These runs used NIST certified sapphire as the reference material. The mass loadings for the runs were 24.8 and 30.3 mg/cm^2, for coal and sapphire, respectively. The raw data from each of these runs was reduced using the first order analysis described previously (the HCAPACITY code). Estimates for the heat capacity of the anthracite char sample derived from each of the runs are plotted in Figure 10. The run-to-run repeatability is within 5% at 400°C. The error is larger at lower temperatures due to larger relative temperature errors.

TABLE II

ANTHRACITE HEAT CAPACITY RUNS

RUN ID	BLANK T (C)	ANTHRACITE T (C)	SAPPHIRE T (C)
1468R19	900	390	440
1468R20	1000	450	520
1468R21	1100	500	560

Results using the complete analysis protocol delineated above applied to anthracite run 1468R21 will now be presented. The initial estimate for anthracite heat capacity is used as input to the full transient, 2-D simulation. Surface plots of the 2-D grid temperature distribution calculated by the transient simulation are given in Figures 11-15 for times of 0.2, 0.4, 0.6, 0.8 and 1.0 sec. One can clearly see the effect that the sample and reference loads have on the local grid temperature. The temperatures in the loaded regions of the grid are hundreds of degrees lower than in the blank regions. These calculations are in qualitative agreement with our observations of numerous heated grid experiments both with the naked eye and the CCD camera based imaging system.

Calculated temperatures at the sample and reference T/C locations are compared with experimental data in Figures 16 and 17 (see lines for original sample heat capacity). The calculated reference temperature is in excellent agreement with experimental data. This is as expected since the model has been calibrated using sapphire as the reference material. The calculated anthracite sample temperature is also in very close agreement with experimental data, but is slightly lower than the measured values at high temperatures. The results indicate that the initial estimate for anthracite heat capacity is somewhat high.

FIG. 10 HEAT CAPACITY OF ANTHRACITE
FIRST ORDER ESTIMATE – THREE RUNS

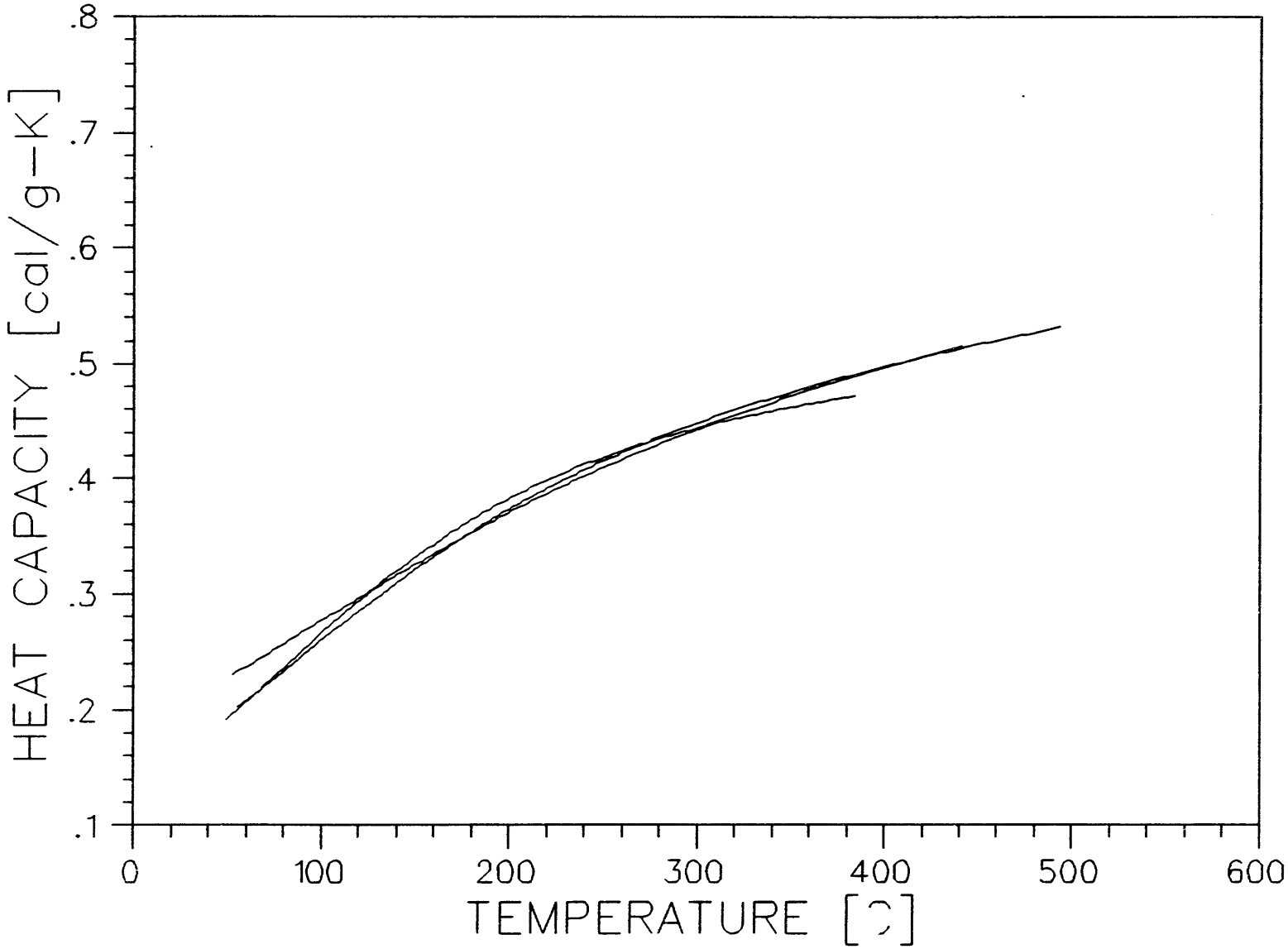

FIG. 11 CALCULATED GRID TEMPERATURE DISTRIBUTION
TIME = 0.20

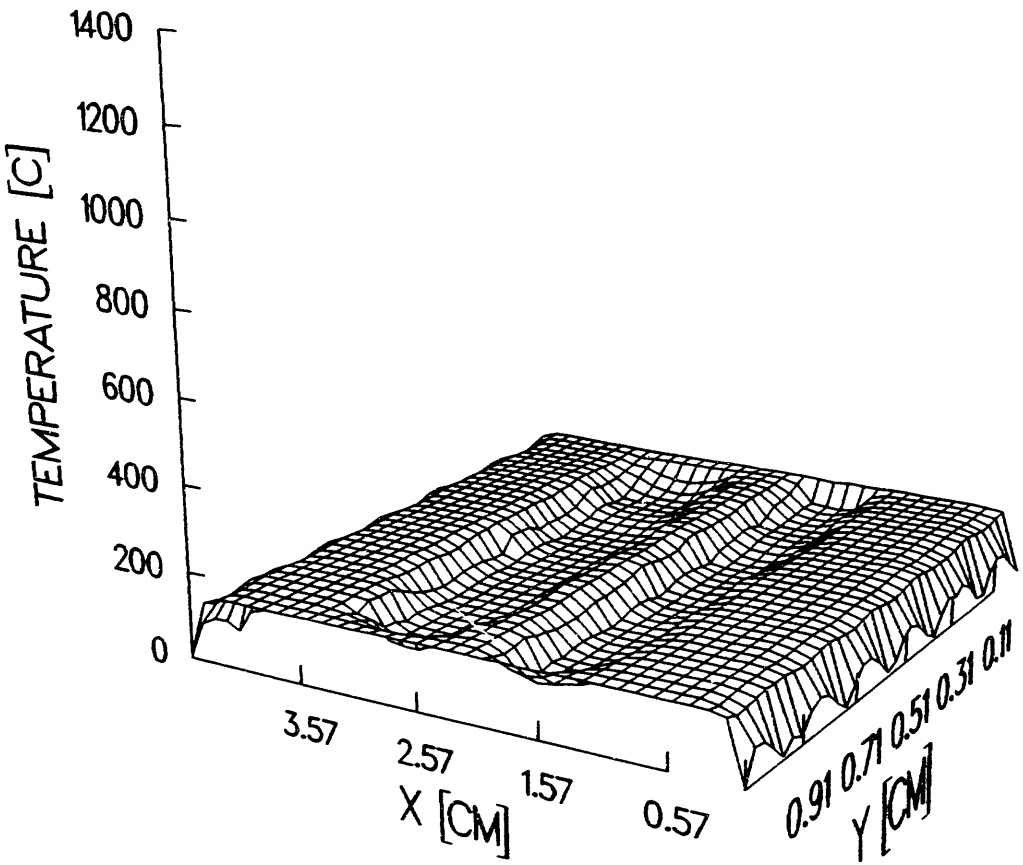

FIG. 12 CALCULATED GRID TEMPERATURE DISTRIBUTION
TIME = 0.40

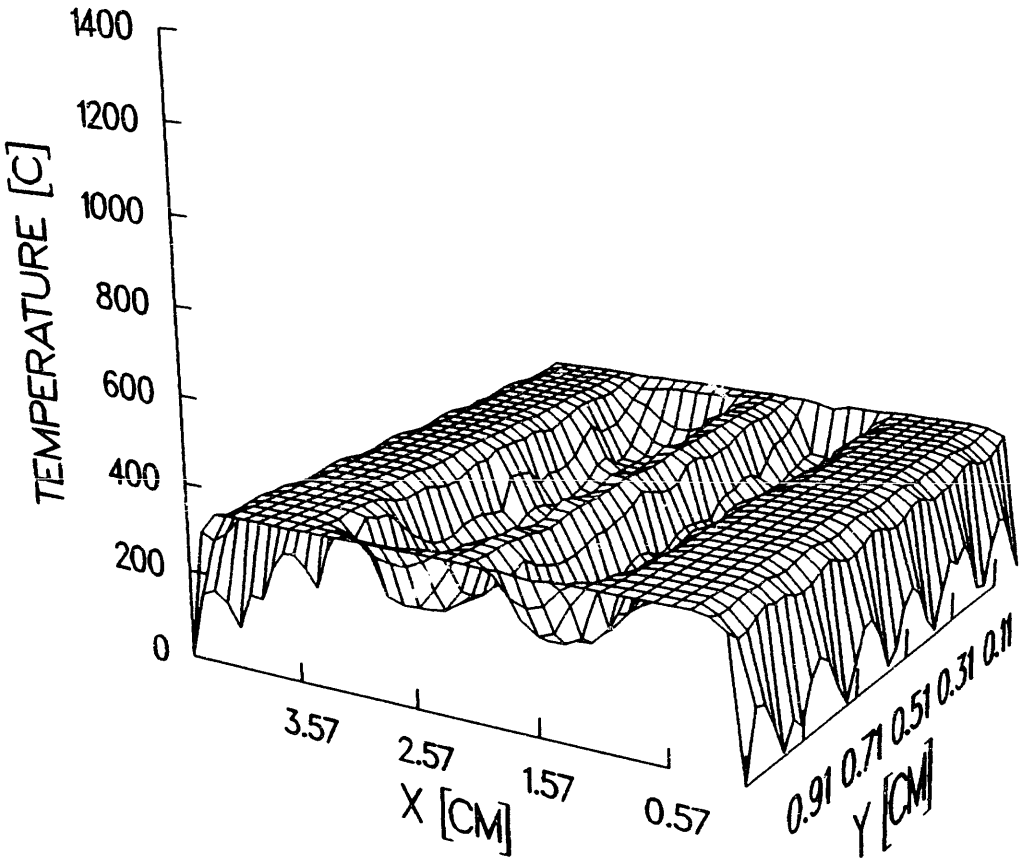

FIG. 13 CALCULATED GRID TEMPERATURE DISTRIBUTION
TIME = 0.60

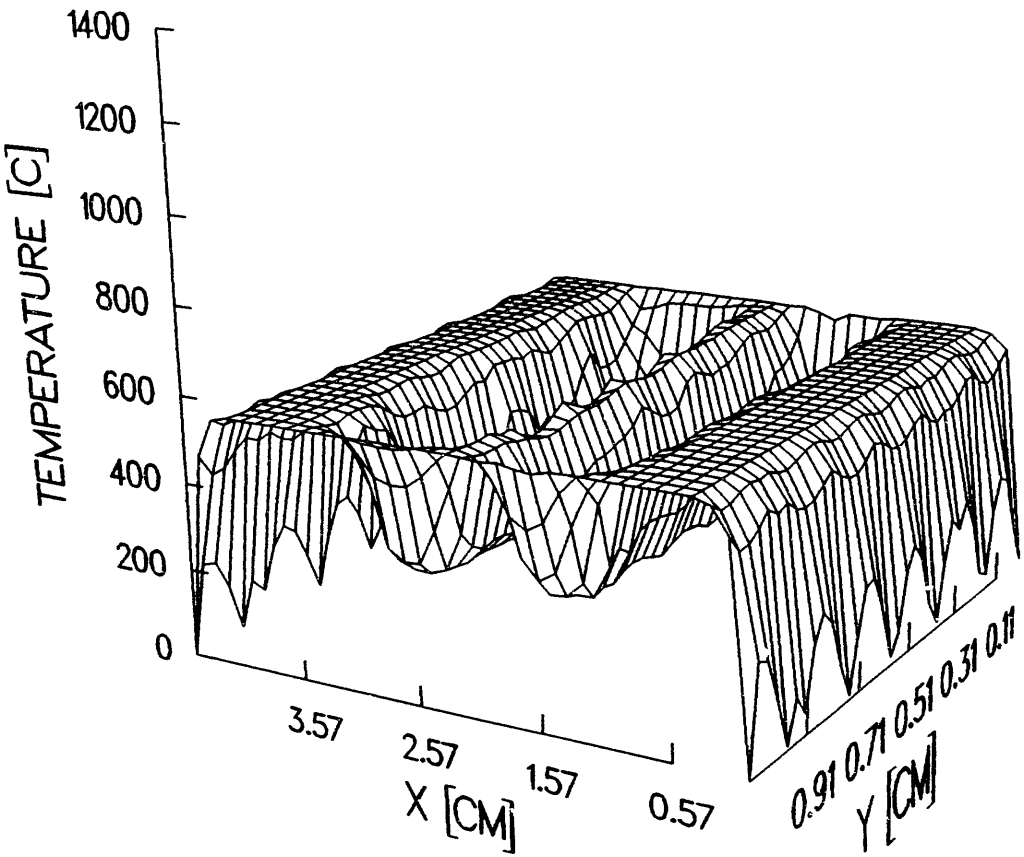

FIG. 14 CALCULATED GRID TEMPERATURE DISTRIBUTION
TIME = 0.80

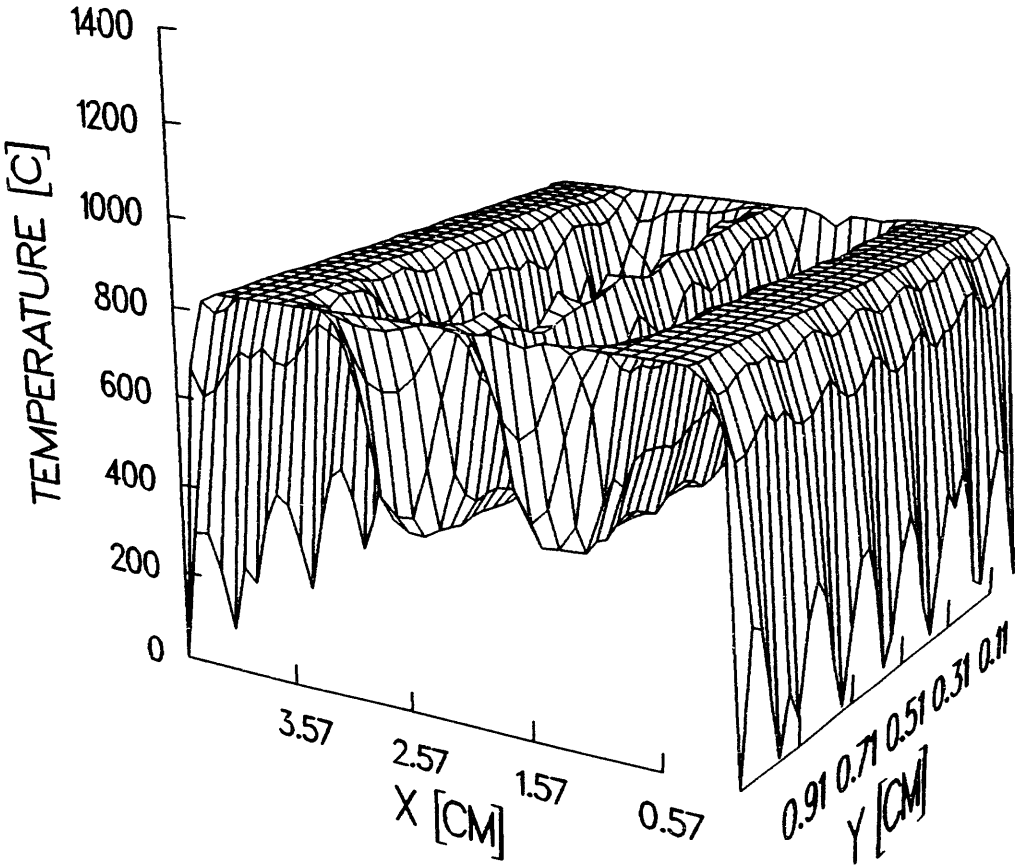

FIG. 15 CALCULATED GRID TEMPERATURE DISTRIBUTION
TIME = 1.00

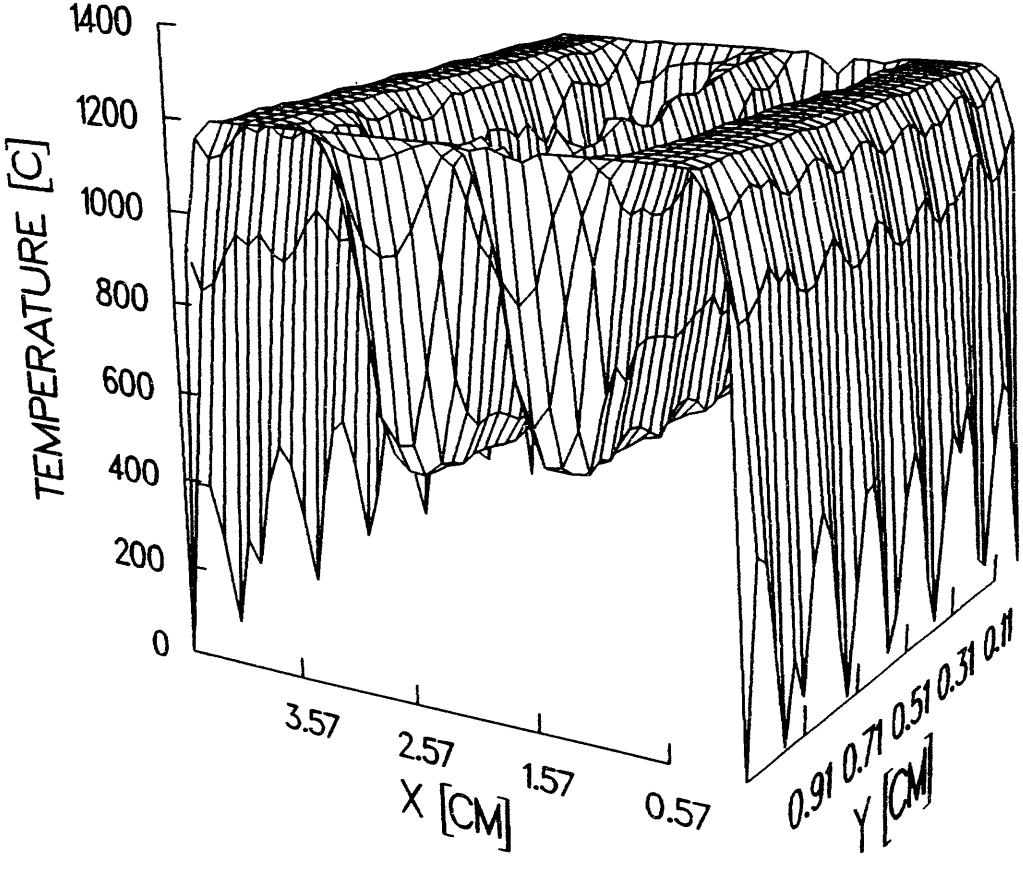

FIG. 16 ANTHRACITE SAMPLE TEMPERATURE CALCULATED (LINES) & EXPERIMENTAL (SYMBOLS)

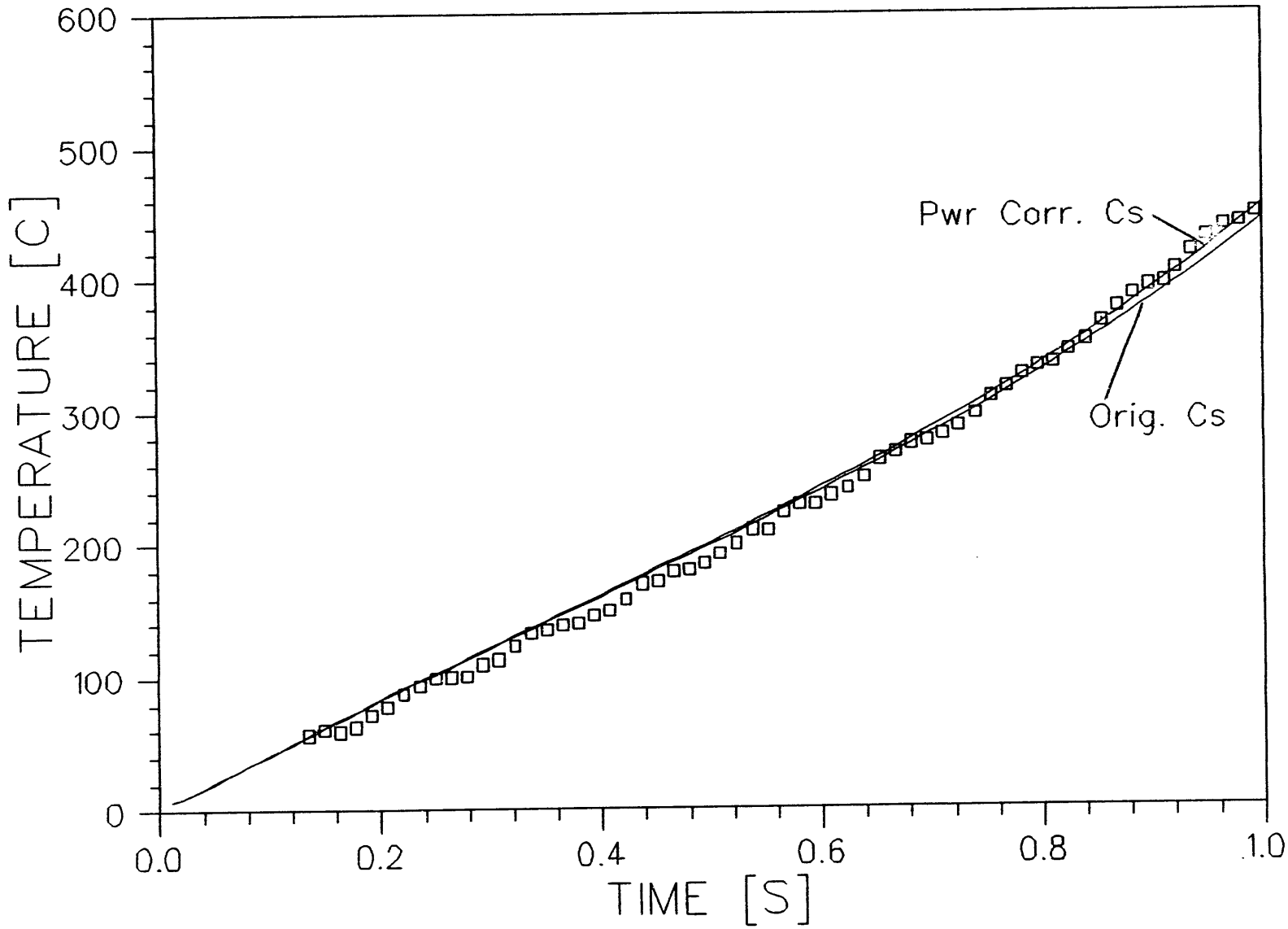

FIG. 17 REFERENCE MATERIAL TEMPERATURE CALCULATED (LINES) & EXPERIMENTAL (SYMBOLS)

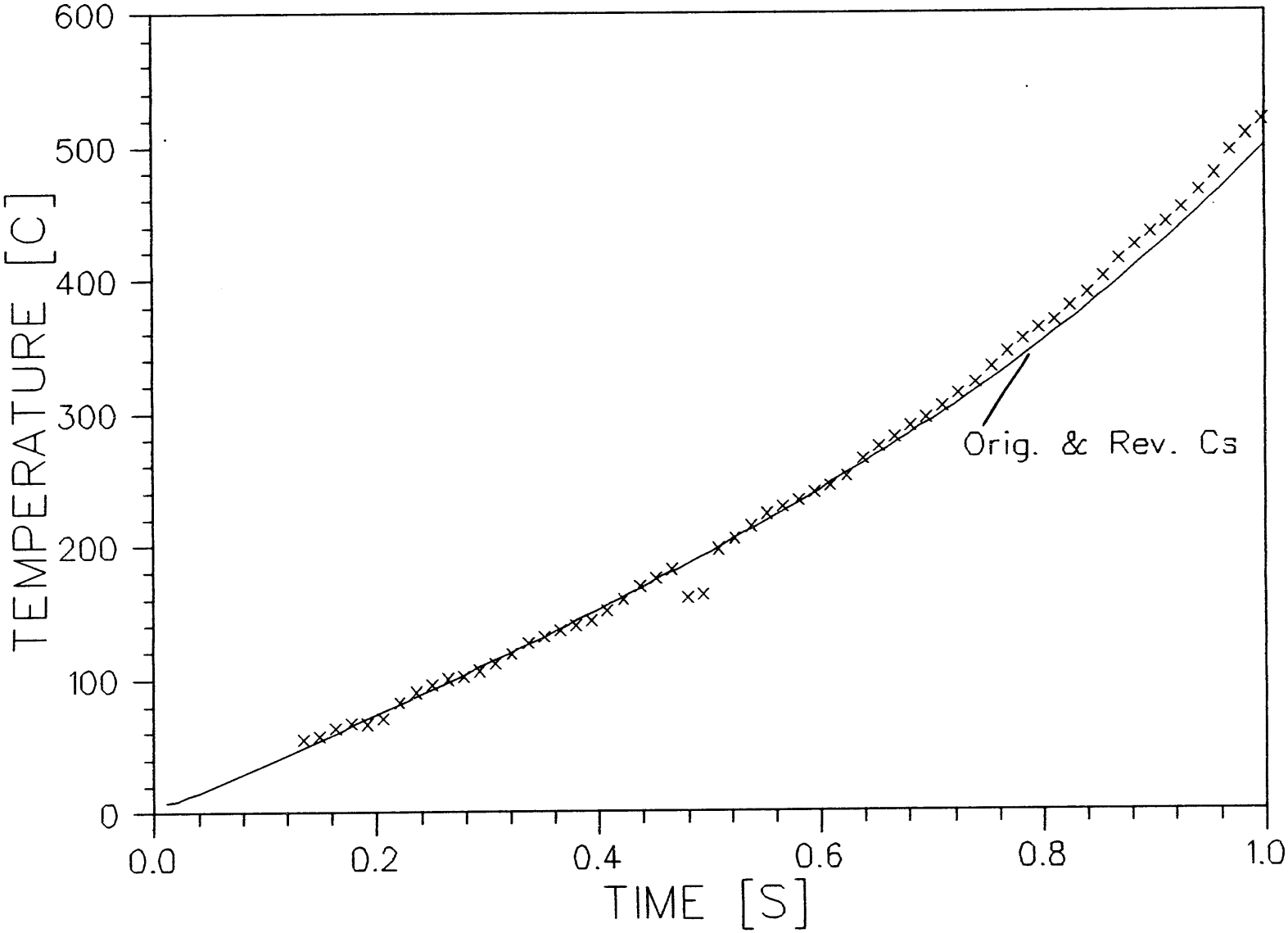

The 2-D code also calculates a corrected sample heat capacity by applying a correction related to the difference in power dissipation between the reference and sample loaded regions of the grid (see equ. 4). The power corrected anthracite heat capacity is compared to the original, first order estimate in Fig. 18.

The 2-D simulation was repeated using the power corrected sample heat capacity curve. The resulting calculated sample and reference temperatures are now in excellent agreement with the experimental temperatures (see lines for revised C_S in Figs. 16 & 17). (The calculated temperatures are within the experimental error of +/- 10°C for the temperature measurements.) The heat capacity analysis protocol has converged on the solution to the heat capacity for the anthracite sample and no further iterations of the procedure are required. The power correction term results in a correction of about 10% to the original, first order estimate for heat capacity. Thus, the power correction is significant and use of this correction improves the accuracy of the heat capacity measurements.

Differential Scanning Calorimeter (DSC) measurements were performed on the anthracite sample in an effort to determine the absolute accuracy of the heated grid heat capacity measurements. Shown in Figure 19, are data from four replicate DSC runs. The measurements were performed by the Polymer Science group at UTRC using a DuPont 9900 DSC. The runs were conducted in a nitrogen atmosphere at a heating rate of 10K/min. The quality of this data is questionable as a result of continuing problems with baseline stability of the DSC cell. The reproducibility of the DSC measurements is very poor, about +/-25%. Also shown in the Figure is the Merrick model (Ref. 7) for heat capacity. The heat capacity measured in the heated grid is bracketed on the low side by the DSC data and on the high side by the Merrick model. Additional, independent, measurements of the heat capacity of the anthracite char sample will be pursued to complete the validation of the high heating rate measurements. Other inert carbon samples will also be examined for their suitability as reference materials.

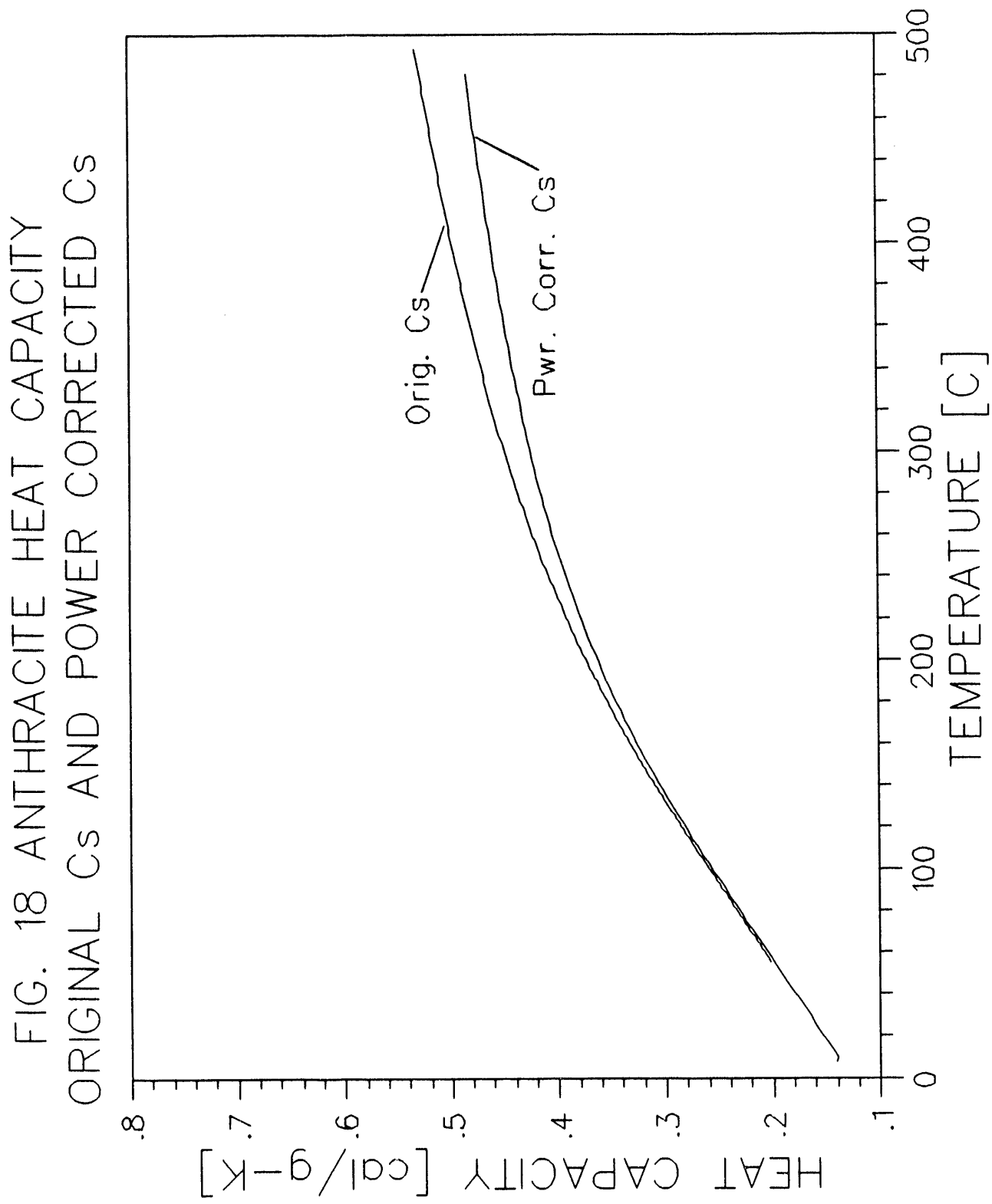
FIG. 18 ANTHRACITE HEAT CAPACITY
ORIGINAL Cs AND POWER CORRECTED Cs
HEAT CAPACITY [cal/g-K]
.8
.7
.6
.5
.4
.3
.2
.1
0
100
200
300
400
500
TEMPERATURE [C]
Orig. Cs
Pwr. Corr. Cs

FIG. 19 ESTIMATE OF ERROR FOR ANTHRACITE Cs
ORIGINAL, POWER CORRECTED AND FOUR DSC RUNS

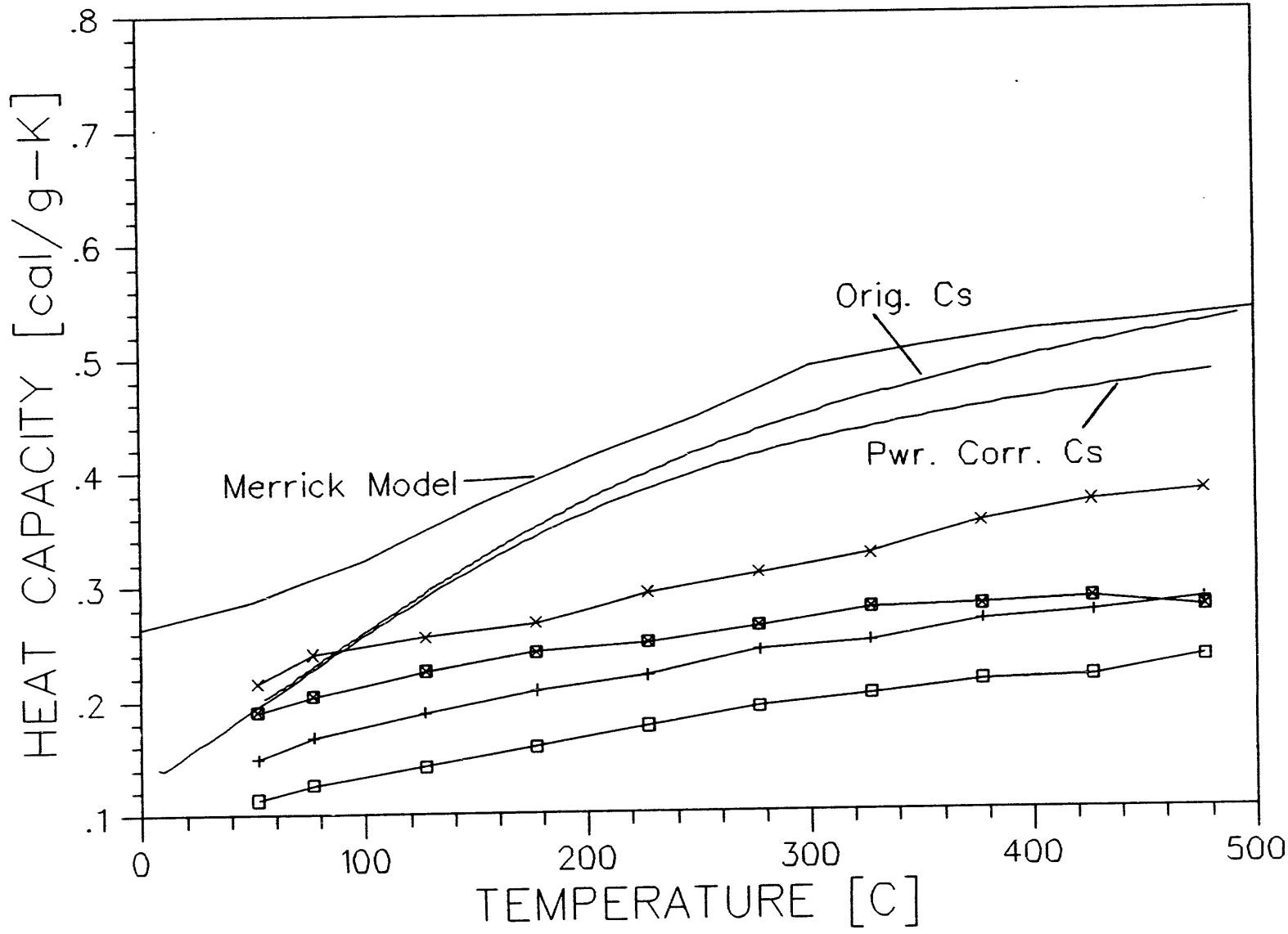

4.0 Task 5. Heat of Thermal Decomposition of Volatile Coal Samples

Generation of Matched Tar and Char Samples

The tar and char samples which are to be used throughout this investigation were generated in the UTRC EFR during this quarter. Matched tar and char samples for PSOC 1451D and 1516D at several extents of reaction have been produced. The quantity of tar and char samples available from each of the runs are:

TABLE III ENTRAINED FLOW REACTOR EXPERIMENTS

Run	Coal Type	Wall Temp. (°C)	Gas Temp. (°C)	Char (g)	Tar (g)
EFR019	1451D	668	507	4.20	0.28
EFR018	1451D	825	660	2.86	0.27
EFR020	1451D	939	796	2.19	0.39
EFR021	1451D	1058	895	2.72	0.28
EFR022	1516D	668	507	4.40	0.07
EFR023	1516D	825	660	1.69	0.07
EFR024	1516D	939	796	1.63	0.08
EFR025	1516D	1058	895	2.29	0.15

It was not possible to save significant quantities of tars from the PSOC 1516D runs due to high static charge. However, sufficient amounts of matched tar and char samples have been produced from PSOC 1451D for use in the performance of this contract.

Elemental analyses of all char samples have been completed. Mass loss values calculated using the ash tracer technique are as follows:

TABLE IV EXTENT OF REACTION OF EFR RUNS

Run	Coal Type	Wall Temp. (°C)	Gas Temp. (°C)	% Mass Loss
EFR019	1451D	668	507	16.7
EFR018	1451D	825	660	31.0
EFR020	1451D	939	796	30.0
EFR021	1451D	1058	895	45.7
EFR022	1516D	668	507	NM *
EFR023	1516D	825	660	8.8
EFR024	1516D	939	796	19.3
EFR025	1516D	1058	895	26.0

* NM - Not Measurable - Volatile yields too low to measure reliably with ash tracer technique. (Mass loss in heated grid experiments at similar final temperature is 5-6%.)

5.0 Planned Activities

Task 2, Calibration of the Heated Grid Calorimeter, is complete although it would be desirable to repeat the DSC measurements for the anthracite char at an independent laboratory. Task 3, Low Temperature Specific Heat Capacity of Volatile Coal Samples will be initiated immediately using PSOC 1451D as the study coal. Task 10, Morphological Characterization, will be performed under subcontract to the University of Pittsburgh. It is expected that the subcontract will be in place early in the upcoming quarter.

6.0 References

1. Fletcher, T.H., *Combustion and Flame*, **78** (2), 223-236 (1989).

2. Best, P.E., et al., *Combustion and Flame*, **66**, 47-56 (1986).

3. Maloney, D.J., et al., *Combustion and Flame*, accepted (1990).

4. Freihaut, J.D., et al., *Combustion Properties of Micronized Coal*, Final Report, DE-AC22-80263, DOE, PETC (1989).

5. Proscia, W.M. and Freihaut, J.D., *Thermodynamic Properties Of Pulverized Coal During Rapid Heating Devolatilization Processes*, Quarterly Report for July-Sept., 1992, DE-AC22-92PC92176, DOE, PETC (1992).

6. Freihaut, J.D. and Proscia, W.M., "Tar Evolution in Heated-Grid Apparatus," *Energy & Fuels*, **3**, 625-635 (1989).

7. Merrick, D., *Fuel*, 62, 534-539 (1983).

APPENDIX A

2-D, TRANSIENT ANALYSIS OF AN ELECTRICALLY HEATED WIRE MESH

UTRC has developed a two-dimensional, transient analysis of a folded, resistively heated wire mesh containing both sample and reference material loaded regions. The analysis is essentially an energy balance calculation which is solved numerically using an implicit algorithm. Given inputs for grid current vs. time, sample and reference material load distributions and estimated sample heat capacity, the code calculates the time-varying temperature distribution for the entire area of the grid. Calculated temperatures at the locations of the sample and reference T/C's are compared to experimentally measured values. The error between the calculated and measured sample temperatures is used to form a corrected sample heat capacity. The validity of the simulation is also checked by comparing calculated grid voltage and power to the experimentally measured values.

Energy Balance

We begin by forming an energy balance for a volume element of an electrically heated wire strand (Nomenclature is defined in Table A-1):

$$E = I^2R - \dot{q}_{cond} - \dot{q}_{env} \tag{A-1}$$

The terms in the energy balance represent, respectively, the enthalpy of the volume element, joule heating, conduction along and across strands, and transfer by radiation and convection to the environment. The enthalpy of the volume element includes the heat stored in both the stainless steel grid and in any sample or reference material mass associated with the grid element,

$$E = \left(m_g C_g + m_s C_s\right) \frac{\partial T}{\partial t} \tag{A-2}$$

The resistance of an elemental length of grid strand is given by the resistivity, length and cross-sectional area of the strand,

$$R = \frac{\rho_e \, dx}{A_x} \tag{A-3}$$

The thermal conduction term includes diffusion of heat in two directions; both parallel and transverse to the current flow,

$$\dot{q}_{cond} = k A_x \frac{\partial^2 T}{\partial x^2} dx + \dot{q}_{y\text{-}dir} \tag{A-4}$$

The conduction in the transverse direction is controlled by two resistances; transfer across the weave contact area to a passive cross strand and conduction along the cross strand,

$$\dot{q}_{y\text{-dir}} = \frac{\Delta T_{y\text{-dir}}}{\frac{\Delta y}{kA_x} + \frac{1}{h_c A_c}} \qquad \text{(A-5)}$$

However, as will be shown below the strand-to-strand contact thermal resistance is small and can be neglected, so that the transverse thermal conduction is given by,

$$\dot{q}_{y\text{-dir}} = kA_x \frac{\partial^2 T}{\partial y^2} dy \qquad \text{(A-6)}$$

Finally, the heat losses to the environment by radiation and conduction are,

$$q_{env} = h_{env} A_{env} (T - T_{env}) \qquad \text{(A-7)}$$

The heat transfer coefficient, h_{env}, is determined empirically and represents the total heat transfer between the actively heated element and its immediate environment.

Now, substituting the expressions for each of the terms into equation (A-1), the energy balance becomes,

$$(m_g C_g + m_s C_s) \frac{\partial T}{\partial t} = I^2R - kA_x \frac{\partial^2 T}{\partial x^2} dx - kA_x \frac{\partial^2 T}{\partial y^2} dy - h_{env} A_{env} (T - T_{env}) \qquad \text{(A-8)}$$

Strand-to-Cross Strand Contact Thermal Conductance

The heat transfer between the actively heated element and its cross-woven strand given by the heat transfer coefficient, h_c, in equation (A-5) will now be discussed. Heat transfer across the interface between two, non-bonded solid surfaces depends on microscopic surface roughness, contact pressure and the thermal conductivity of any interfacial fluid contained in the interfacial voids. The concern in modeling the transient response of a wire mesh consisting of actively heated wire strands "loaded" by the passively heated cross strands is the magnitude of the rate of heat transfer through the inter-strand contact. If h_c is too small then the passive strands will lag the time-temperature profile of the resistively heated strands, significantly complicating the modeling process and the value of the mesh as a component in a thermal analytical instrument. If h_c is sufficiently large, then, in view of the weave geometry, the effect of the presence of passive strands can be modeled by simply doubling the real density of the stainless steel material.

The coefficient h_c contains conductive and radiative components and can be expressed as,

$$h_c = \frac{k_c}{\Delta z} + \sigma\varepsilon^2 f_{rad}^c \left(T^2 + T_{cr}^2\right)\left(T + T_{cr}\right) \qquad \text{(A-9)}$$

where k_c represents the average conduction through the inter-strand contact area, Δz the average separation distance and ε the emissivity or absorptivity of the strand material. Examination of SEM photographs of the wire strands within the mesh reveals that the individual strands are extremely smooth, having a surface "roughness" much less than a micron. Indentations are observed on the strands at the contact points implying that the contact pressure established between the strands during the weaving process is appreciable. These observations indicate that the wire-to-wire gap is submicron in scale length and fairly uniform. A quantitative estimation of the contact area established by the weave pattern has also been made from the SEM photographs.

Calculations to estimate the relative magnitude of h_c indicate that heat transfer across the strand-to-strand contact interface is fast relative to conduction down the cross-strand. The results indicate that the conductance path heat transfer coefficient, irrespective of gas type, is adequate to establish nearly instantaneous thermal equilibrium between the resistive and passive strand volume elements in all conditions except those characteristic of limitations induced by the thermal diffusivity of the strand material itself. Consequently, the simplification given by equation (A-6) above is justified. The "effective " mass of the stainless steel must be doubled to account for the mass of the cross-strands in contact with the x-direction strand.

Empirical Determination of Environmental Heat Losses

The environmental loss heat transfer coefficient, h_{env}, is addressed semi-empirically. As reported elsewhere (Ref. 6), transient and steady state measurements indicate the magnitude of the power dissipation to the environment varies with the thermal conductivity of the ambient gas. Above 600°C, radiation loss dominates the temperature sensitivity of the power loss expression, irrespective of the thermal conductivity of the accompanying gas. With stainless steel electrode clamps, power loss via. electrode conduction is minor compared to the screen surface losses.

The magnitude and temperature dependence of h_{env} has been determined (Ref. 5) under the conditions employed in the grid apparatus for heat capacity measurements. Briefly, the ambient conditions are flowing nitrogen sweep gas and heat losses are determined by measuring the steady state power required to maintain each blank screen temperature and then normalizing with respect to the total environmentally exposed screen surface area. The same h_{env} is used to model

the heat losses from sample loaded elements of the grid, however, the surface area, A_{env}, is modified to account for the additional surface area of the sample exposed to the environment through the open area of the screen weave.

Temperature Dependent Properties

The resistivity, heat capacity and heat loss properties of the stainless steel material vary considerably with temperature. Correlations based on available handbook data and UTRC measurements are used in the model. Given the physical properties of the screen material and the temperature dependence of the heat loss term, the enthalpy requirement of the screen and sample mass dominates the energy balance expression throughout most of the transient heating process at high heating rates.

Numerical Solution Technique

A variable implicitness (in time) solution algorithm has been implemented. All calculations reported here used an implicitness factor of 1/2. This is a centered or Crank-Nicholson scheme which is unconditionally stable and second-order accurate in time. The implicit algorithm was necessary to obtain stable solutions for sample loaded grid calculations. The steep temperature gradients at the edge of a sample loaded region of the screen impose severe requirements on the solution algorithm. The earlier version of the code used an explicit technique to model blank screens, but required prohibitively small time steps to maintain numerical stability.

TABLE A-I

NOMENCLATURE

A_x = cross-sectional area of a grid strand, [cm^2]

A_c = contact area between current carrying strand and cross strand, [cm^2]

C_g = heat capacity of 304 stainless steel, [J/gm-K]

C_s = heat capacity of sample, [J/gm-K]

dx = length of grid element in discretization, [cm]

dy = width of grid element in discretization, [cm]

ε = emissivity = absorptivity of 304 stainless steel

f^c_{rad} = radiative view factor for strand to cross-strand contact area

h_c = strand-to-cross-strand heat transfer coefficient, [J/s-cm^2-K]

h_{env} = heat transfer coeff. for conductive and radiative losses, [J/s-cm^2-K]

I = grid current, [amp]

k = thermal conductivity of 304 stainless steel, [J/s-cm-K]

k_c = contact conductance between current carrying strand and cross strand, [J/s-cm-K]

m_g = grid mass per elemental volume, [gm]

m_s = sample mass per elemental volume, [gm]

R = electrical resistance of grid strand of length dx, [ohm]

ρ_e = resistivity of 304 stainless steel, [ohm-cm]

σ = Stefan-Boltzmann constant, [J/s-cm^2-K^4]

T = temperature of grid strand and associated sample, [K]

T_{env} = temperature of ambient environment, [K]

T_{cr} = temperature of cross-strand, [K]

x = direction parallel to current flow in grid, [cm]

y = direction perpendicular to current flow in grid, [cm]

END

DATE
FILMED
6/16/93